Proceedings of the American Control Conference
Albuquerque, New Meixco June 1997
0-7803-3832-4/97/$10.00 © 1997 AACC

Lane Following During Backward Driving for Front Wheel Steered Vehicles

Satyajit Patwardhan, Han-Shue Tan, Jürgen Guldner
CALIFORNIA PATH,
UNIVERSITY OF CALIFORNIA AT BERKELEY,
INSTITUTE OF TRANSPORTATION STUDIES, BLDG. 452
1357 S 46TH STREET, RICHMOND CA 94804-4698

Masayoshi Tomizuka
DEPARTMENT OF MECHANICAL ENGINEERING,
UNIVERSITY OF CALIFORNIA AT BERKELEY,
ETCHEVERY HALL, BERKELEY CA 94720

Abstract

This paper addresses the problem of automatic backward driving of passenger vehicles following a specified path. Additional difficulties associated with backward driving, as compared to forward driving are pointed out, with special attention to the sensor location. A special controller structure, based on a concept of kinematic linkage is proposed to overcome the dynamic difficulties associated with backward driving. Simulations and experiments demonstrate its performance and functionality.

I. Introduction

The need of backward driving is encountered in several application areas. The most frequent application is automatic guidance of self powered cargo moving vehicles (AGV, the Automatically Guided Vehicles)[1]. Such cargo moving vehicles have to navigate themselves on a crowded shop floor or in a warehouse. Often, there is not enough space for the AGV to turn around and the vehicle has to perform backup operation[1]. In addition, the need for backward driving has also been identified in some scenarios of intelligent vehicle highway systems (IVHS)[2]. For relieving traffic congestion, caused by an accident in IVHS, the vehicles sufficiently upstream of the incident will be notified well in advance and will be diverted to alternate routes or to neighboring clear lanes if available. However, there may be large number of vehicles trapped immediately behind the obstacle produced by the accident. In order for these vehicles to leave the blockade, they should either (i) change lane or (ii) drive backwards to the nearest exit point upstream. In the later case, the need for backward driving algorithm is quite clear. In the former case, the vehicles that are trapped at zero velocity, need to perform backward driving in order to gain sufficient maneuvering space for lane change [2].

The problem of automatic guidance for forward driving has received considerable attention by several research groups in the past. Some examples are electric wire guidance, first tested at OSU[3] and later by Daimler-Benz[4], and magnetic markers used in the California PATH program[5] and, most recently, in Japan[6]. In addition, several US and international patents have also been issued on the subject. On the other hand, because of somewhat smaller application domain, the problem of backward driving has received much less attention in the IVHS research community. The only available literature comes from the areas of AGV or mobile robots [2].

This paper aims at addressing the problem of backward driving by explaining the difficulties from the control viewpoint and proposing a solution to the problem. First, a model for backward driving is presented in section II. The proposed lane following controller for backward driving, along with the issues of stability, performance tradeoffs, road curvature effects and extension to articulated vehicles will be presented in section III. Simulation study of the system will follow in section IV and experimental results in section V. Finally, conclusions and future direction of research will be presented in section VI.

II. Difficulties in Backward Driving of Front Steered Vehicles

2.1 Vehicle Model

Consider a kinematic model for a car (Fig 1). Although simplistic, this model does retain fundamental problems involved in controlling the vehicle in backward direction. Without loss of generality, the road is assumed to be straight and along X axis.

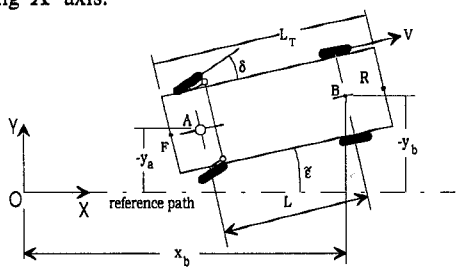

Figure 1: Kinematic car model

From Fig. 1, differential equations of motion with no-slip assumption can be written as

$$\dot{x}_b = V\cos(\tilde{\varepsilon}),\ \dot{y}_b = -V\sin(\tilde{\varepsilon}),\ \dot{\tilde{\varepsilon}} = \frac{-V\tan(\delta)}{L} \qquad (1)$$

Table 1: Definition of Variables

Name	Description
x_b	X coordinate of midpoint of rear axle.
y_b	Lateral displacement w.r.t. road center at rear axle
y_a	Lateral displacement w.r.t. road center at front axle
$\tilde{\varepsilon}$	Relative yaw angle of vehicle w.r.t. road centerline
δ	Steering angle
V	Vehicle speed (measured positive in backward direction)
L	Wheel base
L_T	Car length

2.2 Model Analysis

The aim of the controller is to make a chosen point (along the vehicle axis of symmetry), track the road centerline with small tracking error. In addition, the *yaw* dynamics of the vehicle should be stable and *relative yaw* should be bounded by a small number. The available control input is front wheel steering angle. We take a brief look at the system dynamics for forward driving in order to understand the differences between forward and backward driving.

In forward driving with a look-down sensing scheme, the measurement of lateral displacement is made at a point in front of the vehicle center of gravity[7], typically at the front axle (y_a). In addition, an alternate sensing point can be located at the rear axle of the vehicle(y_b). Based on Eq. (1), the transfer functions from steering angle δ, to y_a and y_b are

$$F_{\delta\to y_a}=\frac{y_a(s)}{\delta(s)}=V\frac{sL+V}{s^2L},\ F_{\delta\to y_b}=\frac{y_b(s)}{\delta(s)}=\frac{V^2}{s^2L} \qquad (2)$$

It can be seen that $F_{\delta\to y_a}$ has two poles at the origin that come from the chain of two integrators, one from steering angle to yaw angle and the other from yaw angle to lateral displacement. In addition, $F_{\delta\to y_a}$ has a stable zero at $\frac{-V}{L}$. As for $F_{\delta\to y_b}$, the two poles at the origin remain the same, but it does not have any zero.

Now, consider the backward driving situation. The corresponding transfer functions are

$$R_{\delta\to y_a}=\frac{y_a(s)}{\delta(s)}=-V\frac{sL-V}{s^2L},\ R_{\delta\to y_b}=\frac{y_b(s)}{\delta(s)}=\frac{V^2}{s^2L} \qquad (3)$$

In contrast to the forward driving situation, $R_{\delta\to y_a}$ has an *unstable* zero at $\frac{V}{L}$ and the same double pole at the origin. $R_{\delta\to y_b}$ still has the origin pole pair, but no zero. Figure 2 shows root loci for the backward and forward driving.

Fundamental differences between forward and backward driving can be seen from Fig. 2. Kinematically, when the sensor at the front axle is used for control, a simple proportional controller will suffice for forward driving. In reality, additional lead will have to be provided by the controller to compensate for the vehicle side slip dynamics and actuator lag.

On the contrary, for backward driving using a front axle sensor, a simple proportional controller will not be sufficient. Certainly the non-minimum-phase zero at V/L can not be canceled with an unstable controller pole. Thus, in order to stabilize the system, quite elaborate arrangement of zeros and poles will have to be introduced by the controller. For example a stable zero pair (along with a pair of fast poles to realize the zero pair) will have to be introduced to attract the root loci emanating from the double pole at the origin. However, the system tuning will be quite tricky and the system will be only conditionally stable, because the root loci have to enter the right half plane eventually to meet the unstable zero. The overall system gain has to be such that the closed loop poles do not appear in the right half plane. Since the vehicle gain depends on speed and tire-road interaction, the system would have poor robustness properties. The second alternative is to use a sensor at the rear axle for controlling the car. This is a much better alternative. However, the controller will have to introduce sufficient phase lead to stabilize the simple kinematic double integrator. The required lead will be even more if one takes into account the actuator lag and high speed side slip dynamics.

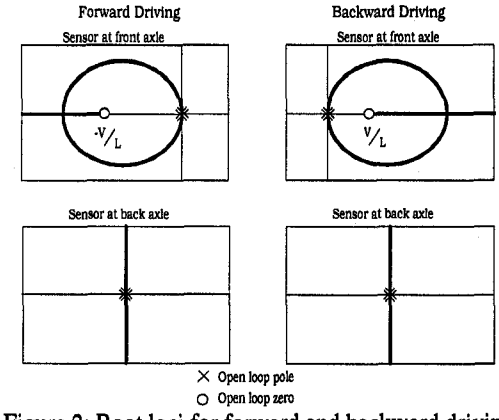

Figure 2: Root loci for forward and backward driving

III. Lane Following Controller for Backward Driving

3.1 Controller Mechanism

As discussed in the previous section, the choices of front or rear axle sensors are not very attractive from the control viewpoint. In order to devise a good control strategy, intuition was gained by observing the way humans navigate a boat that has a rudder at the rear end. A boat with the rudder is kinematically similar to a car driven backwards. Inspired by this similarity, a controller in the form of a mechanism is proposed as shown in Figure 3.

The mechanism can be implemented either in software or in hardware. If implemented in hardware, it will serve as a steering gear for human controlled cargo vehicles that have steering wheels at the rear. In case of IVHS, this mechanism will be embedded purely in software that controls the steering wheels. The mechanism consists of a long link D of length $(a+b)$, which is hinged at the midpoint of the rear axle. One end of this link is made to follow the road centerline and the other end carries a pin that slides along the link E, to which the steering wheels are made to be parallel. The mechanism works as follows. Consider a situation shown in Fig. 3. One can observer three facts about the mechanism: (i) when the car starts moving in the backward direction, the steering wheels are always pointed such that the car tends to align itself with the link D; (ii) once aligned with D, the car moves in the direction pointed by the link D and (iii) the link D always points towards

the lane centerline. Based on these three observations, convergence to the reference path and hence the closed loop stability follows intuitively. The analytical stability proof is given in next section.

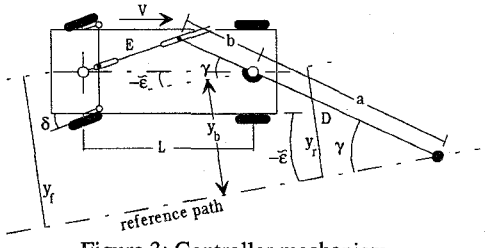

Figure 3: Controller mechanism.

In order to realize the mechanism, the vehicle states have to be measured. In the following discussion, it is assumed that the vehicle is equipped with look-down sensors at front and rear bumpers. However, the application of the mechanism of Fig. 3 is not limited to this sensing scheme. In case of alternate sensing schemes such as vision, the *relative yaw* angle $\tilde{\varepsilon}$, can be directly measured and need not be computed from the front and the rear lateral displacements. The set of equations defining the controller will slightly change depending on the sensing scheme. From Figs. 1 and 3, for look-down sensing, one can write the control law as

$$\delta = \tan^{-1}\left(\frac{b\sin(\gamma+\tilde{\varepsilon})}{L-b\cos(\gamma+\tilde{\varepsilon})}\right) \tag{4}$$

where, $\sin(\gamma) = \frac{-y_b}{a}$ $\tan(\tilde{\varepsilon}) = \frac{y_f - y_r}{L_T}$ $y_b = y_r + \frac{l_r}{L_T}y_f - \frac{l_r}{L_T}y_r$

Equation (4) is a non-linear equation that defines the controller. Assuming that the angles γ, $\tilde{\varepsilon}$ and δ are small, Eq. (4) reduces to the linear control law

$$\delta = \frac{b}{a(L-b)}\left[-y_r + \frac{a-l_r}{L_T}(y_f - y_r)\right] \tag{5}$$

3.2 Stability Analysis

Two aspects of stability analysis will be discussed in this section: (i) the stability of the equilibrium points and (ii) the associated domains of attraction for the stable equilibrium points. The first step is to find the equilibrium points of the nonlinear closed loop system given by Eqs. (1) and (4). Combining them yields

$$\frac{d}{dt}\begin{bmatrix} y_b \\ \tilde{\varepsilon} \end{bmatrix} = f(\mathbf{X}) = \begin{bmatrix} -V\sin\tilde{\varepsilon} \\ \dfrac{Vb\sin(\sin^{-1}(y_b/a)-\tilde{\varepsilon})}{L(L-b\cos(\sin^{-1}(y_b/a)-\tilde{\varepsilon}))} \end{bmatrix} \tag{6}$$

where $\mathbf{X}$ is the state vector defined as

$$\mathbf{X} = [y_b \quad \tilde{\varepsilon}]^T \tag{7}$$

It can be readily seen that the equilibrium points of Eq. (6), given by $f(\mathbf{X}) = 0$ are $y_b = 0, \tilde{\varepsilon} = n\pi, n = \ldots,-2,-1,0,1,2,\ldots$

When linearized around the equilibrium points $\tilde{\varepsilon} = 0, y_b = 0$ and $\tilde{\varepsilon} = \pi, y_b = 0$ the system Jacobians are:

$$\mathbf{J}(0,0) = \frac{d}{d\mathbf{X}}f(\mathbf{X})\Big|_{\tilde{\varepsilon}=0,y_b=0} = \begin{bmatrix} 0 & -V \\ \dfrac{Vb}{aL(L-b)} & \dfrac{Vb}{L(L-b)} \end{bmatrix}$$

$$\mathbf{J}(\pi,0) = \begin{bmatrix} 0 & V \\ -\dfrac{Vb}{aL(L+b)} & \dfrac{Vb}{L(L+b)} \end{bmatrix},$$

with eigenvalues as in Table 2.

Table 2. Equilibrium Points and Eigenvalues

Equilibrium point	Eigenvalues
$\tilde{\varepsilon} = 2n\pi, y_b = 0;$ $n = 0,\pm1,\ldots$	$\frac{V}{2}\left(\frac{ab \pm \sqrt{a^2b^2 - 4abL(L-b)}}{-aL(L-b)}\right)$
$\tilde{\varepsilon} = (2n-1)\pi,$ $y_b = 0; n = 0,\pm1,\ldots$	$\frac{V}{2}\left(\frac{ab \pm \sqrt{a^2b^2 - 4abL(L+b)}}{aL(L+b)}\right)$

Figures 4 and 5 show the variation of the eigenvalues with respect to a and b for the equilibrium points $(\tilde{\varepsilon} = 2n\pi, y_b = 0)$ and $(\tilde{\varepsilon} = (2n-1)\pi, y_b = 0)$ respectively.

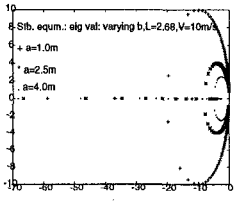

Figure 4

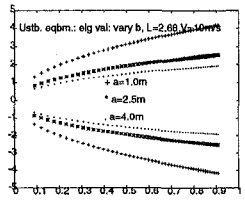

Figure 5

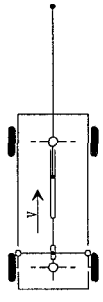

Stable Equilibrium

Figure 6a

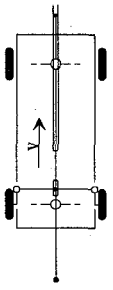

Unstable Equilibrium

Figure 6b

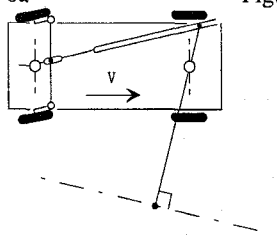

Mechanism in Locked Position

Figure 6c

For $a > 0$ and $0 < b < L$, one can see that the equilibrium points $(\tilde{\varepsilon} = 2n\pi, y_b = 0)$ are always stable. On the other hand for the same range of a and b, the equilibrium points $(\tilde{\varepsilon} = (2n-1)\pi, y_b = 0)$ are unstable. In fact, with the controller mechanism of Fig 3, the backward driving closed loop transfer function around the stable equilibrium point looks much like the one for forward driving with front axle sensor (compare Fig. 4 and Fig. 2). The car and the controller mechanism configurations for stable and unstable equilibrium points are shown in Fig. 6.

The next step in the stability analysis is to find the domains of attraction for the stable equilibrium points. This is achieved by numerical analysis. The state plane of the system is carefully analyzed using numerical simulations. The results are shown in Figs. 7 and 8. These figures are drawn for two different configurations of the mechanism applied to the same car. The trajectories drawn in these figures are trajectories emanating

from the ten points: $(\tilde{\varepsilon} = \pm n\pi, y_b = \pm a)$, $n = -2,-1,0,1,2$; when Eq. (6) is run forward and backward in time. Some of these trajectories (solid lines) divide the state space into several regions.

As marked, the region $(|y_b| > a)$ is impossible to reach because y_b can not be bigger than a. The remaining portion of the state plane $(|y_b| \le a)$ is further subdivided into regions, whose meaning is as follows.

Origin Stable, $(2\pi,0)$ Stable, $(-2\pi,0)$ Stable — The mechanism will eventually align itself with the road centerline (stable configuration of Fig. 6a) if the initial configuration lies in any of these three regions. Depending on the region of the initial condition, the mechanism will converge to either (0,0), or $(2\pi,0)$ or $(-2\pi,0)$. Physically, these three equilibrium points are equivalent. The difference lies whether the car takes a full $\pm 360^0$ turn before reaching the equilibrium or not.

Lock — The car and the control mechanism will reach the locked position shown in Fig 6c. Once in this configuration, the vehicle will stop moving because of the constraints imposed by the link lengths.

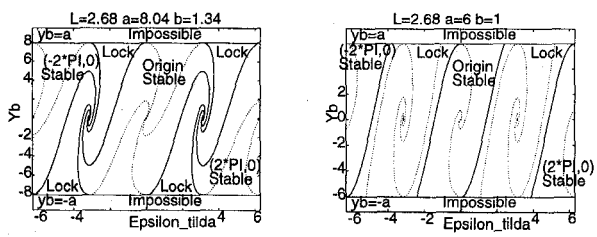

Fig 7,8: State plane analysis

The phenomenon of locking is present if the mechanism is realized by physical links or the full non linear control law of Eq. (4) is used. In the latter case, when in the locked position, the controller will attempt to find out arcsin of a number bigger than 1. If the mechanism is realized in software, the controller can be forced to pass through the locked position by assigning

$$\gamma = \begin{cases} \sin^{-1}(-y_b/a) & \forall \quad |-y_b/a| \le 1 \\ \pi/2 & \forall \quad -y_b/a > 1 \\ -\pi/2 & \forall \quad -y_b/a < -1 \end{cases} \tag{8}$$

This situation has only academic interest, because by this time the car is already at a distance of several car lengths away from the road centerline and the lateral sensors would have stopped sensing the lateral position by this time.

3.3 Performance Tradeoffs

The link lengths a and b are the design parameters. As shown in section 3.2, for asymptotic stability, a and b have to be in the following range.

$$0 < a < \infty, \quad 0 < b < L \tag{9}$$

The variation of closed loop damping coefficient with a and b is shown in Figure 9.

To understand the effects of a and b on the performance, consider Eq. (5). It can be noticed that the parameter b purely affects the controller gain. In fact, the controller gain goes from $+\infty$ to 0 when b varies from L to 0. Consequently, the tracking accuracy deteriorates and ride quality improves, primarily because of reduction in high frequency gain, with decrease in b. In addition, the damping improves with increasing b as shown in Fig. 9.

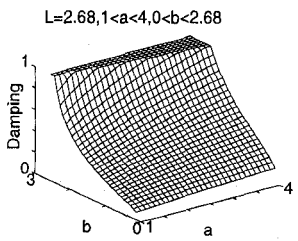

Figure 9. Closed loop damping.

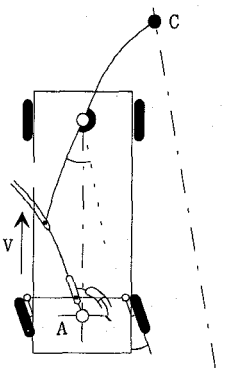

Figure 10: Mechanism with damper and flexible links.

The most important effect of the parameter a is seen by observing that the difference between the lateral error at front and rear end of the car is multiplied by $(a - l_r)$ in Eq. (5). In addition, a also appears in the denominator of overall controller gain. Effectively, with increase in a, the low frequency gain of the controller reduces while keeping the high frequency gain about the same. In the process, the mid frequency phase lead increases. Conceptually, this projects the lateral error at a distance a away from the car and tends to increase the high frequency gain. But the tracking point is also projected ahead, and tends to reduce the overall gain. These two effects counteract each other in the high frequency range. The parameter a determines the amount of lead provided by the controller, by determining the projection distance. Thus, increase in a increases the stability margin and damping of the system (see Fig. 9). On the other hand, with increase in a, the high frequency gain of the controller increases as compared to the low frequency gain (the relative proportions of y_r and $(y_f - y_r)$ are affected by a). In turn, the high frequency noise in lateral sensors will be amplified with increase in a if the low frequency gain is kept constant, by adjustment of b to satisfy the steady state tracking accuracy requirements. The third effect of the parameter a, which is not obvious from Eq. (5), is the preview distance. This effect will be discussed in the next section.

If the freedom provided by choice of a and b is not sufficient for a good compromise between ride quality and tracking error, the links of the mechanism can be made flexible and a damper can be added at the steering wheels as shown in Figure 10.

Let the effective stiffness from point A to C be k Nm/m and the damping at the steering wheels be c Nm/(rad/s). The additional flexibility and damping introduce a first order low pass filter with transfer function of $\frac{k}{sc+\frac{ka}{b}(L-b)}$ in the control law given by Eq. (5). This arrangement can effectively filter out high frequency noise without sacrificing the steady state error.

3.4 Road Curvature and Preview

Until now, the road was considered to be straight. This treatment is adequate for the stability analysis. However, if the road curvature information is available, as in case of magnetic marker roadway reference systems[5], one can incorporate the information into the mechanism to improve the tracking performance on curves, without sacrificing ride comfort. As shown in Fig 11, the proposed controller provides an obvious way to do so.

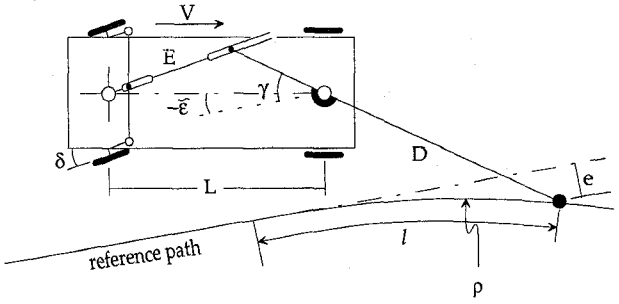

Figure 11. Road curvature effect.

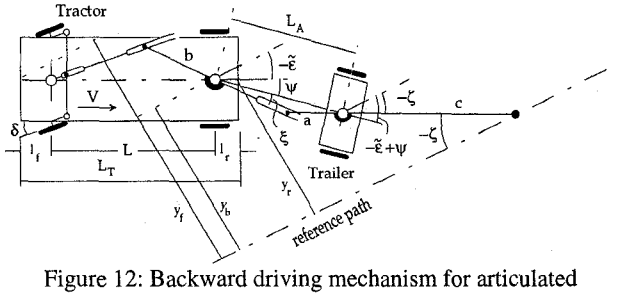

Figure 12: Backward driving mechanism for articulated vehicles

The quantity e, defined in Fig 11, modifies Eq. (4) as follows.

$$\sin(\gamma) = \frac{-y_b + e}{a} \tag{10}$$

where

$$e = \rho(1 - \cos(l/\rho)) \tag{11}$$

Since the curvature is a second order effect, Eq. (11) can be simplified for implementation by expanding up to second order terms to yield

$$e = \frac{l^2}{2\rho} \tag{12}$$

If there are n different curvatures $\rho_1, \cdots, \rho_n$, each lasting for $l_1, \cdots, l_n$ meters of the roadway within the preview length, then

$$e = \sum_{i=1}^{n} \frac{l_i^2}{2\rho_i} \tag{13}$$

3.5 Extension to Articulated Vehicles

The backward driving mechanism can be extended to work for articulated vehicles. This is a very interesting problem with possible application to guiding the airplane pushing vehicles when airplanes are pushed from terminals to taxiways. However, this problem will not be fully discussed in this paper. Only the basic idea of extension will be presented without the detailed analysis.

We consider a tractor-trailer vehicle with one articulated joint. As in the case of non-articulated vehicles, our goal is to make a suitable point (along the longitudinal axis of symmetry) of each of the tractor and the trailer to follow the desired path with small tracking error. Also, the *relative yaw* ($\tilde{\varepsilon}$) and the *angle of articulation* (ψ) should converge to small numbers. The proposed mechanism is presented in Figure 12. This mechanism translates into the following control law.

$$\delta = \tan^{-1}\left(\frac{b\sin(\psi+\xi)}{L - b\cos(\psi+\xi)}\right) \tag{14}$$

where

$$\tan\xi = \frac{a\sin(\psi - \tilde{\varepsilon} + \zeta)}{L_A - a\cos(\psi - \tilde{\varepsilon} + \zeta)}$$

$$\sin\zeta = \frac{y_b - L_A\sin(\psi - \tilde{\varepsilon})}{c}$$

$$y_b = y_r + \frac{l_r}{L_T}y_f - \frac{l_r}{L_T}y_r$$

and

$$\tan\tilde{\varepsilon} = \frac{y_f - y_r}{L_T}$$

Assuming that δ, ξ, ζ and $\tilde{\varepsilon}$ are small, the control law can be simplified to

$$\delta = \frac{b}{(L-b)(L_A - a)cL_T}[(aL_A + al_r - ca)y_f + (ca + L_T a - aL_A - al_r)y_r + (c-a)L_T L_A \psi] \tag{15}$$

The stability of this arrangement is guaranteed only for certain proportions of link lengths. The discussion on the link length constraints for stability is deferred as part of future work.

IV. Simulation Study

Simulations of backward driving of non articulated vehicles using the control law (6) were performed for the parameters of a PATH test vehicle, a PONTIAC 6000STE. The vehicle and controller parameters were L=2.68, $L_r = 4.45$, $l_r = 0.91$, a=6.0, $b = 1.0$ (everything in meters). Figures 13 shows the results of simulation when the vehicle speed is 10m/s (22.5mph) and the initial condition is $y_b = 0.3$m and $\tilde{\varepsilon} = -5^o$. The figure provides the time history of y_b, $\tilde{\varepsilon}$ and δ as well as the response in the state plane. As seen in the figures, the vehicle state converges to the origin of the state plane and the closed loop system is asymptotically stable.

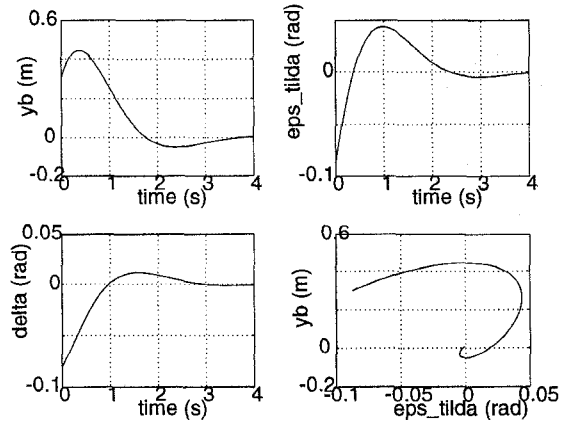

Figure 13: Vehicle time history and state plane

V. Experimental Verification

The experimentation on the PONTIAC 6000STE test vehicle was conducted on the test track at the Richmond Field Station of the University of California at Berkeley. The track consists of a series of 11 curves as shown in bottom left plot of Figure 14. The vehicle and controller parameters were as stated in the previous section, and the vehicle speed was 7.8m/s (@17mph). As seen in Fig. 14, the tracking error is within ±25cm, both at the front and the rear bumpers. A maximum speed of 13.33m/s (30mph) was achieved without road preview for backward driving. These results verify that the control law inspired by the kinematic considerations performs well at relatively low speeds.

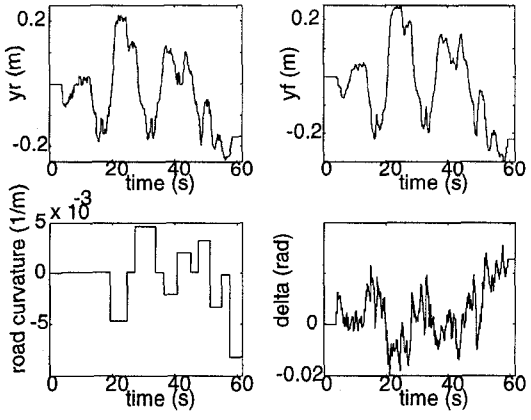

Figure 15: Experimental results

VI. Conclusions

This paper addressed the problem of backward driving. Fundamental difficulties associated with backward driving were pointed out using a kinematic model. A linkage inspired controller was proposed to solve the problems associated with backward driving. The effectiveness of the controller was demonstrated by simulation and experimentation. The linkage controller provides a natural solution to the difficult problem of backward driving. This solution serves as a baseline control design, from which more sophisticated control laws can be developed. Our future research will address the additional problems associated with high speed driving with the actuator dynamics and the vehicle side slip dynamics, which are significant for high speed driving.

Acknowledgment

This work was performed as part of the *Partners for Advanced Transit and Highways (PATH)* program, prepared under the sponsorship of the State of California, Transportation and Housing Agency; Department of Transportation (CalTrans).

We would like to express our sincere thanks to Dr. S. Shladover and Mr. W. Zhang of California PATH for their insightful comments and suggestions.

References

[1] T. Blakeslee, "Reverse Direction Guidance System for Lift Truck", United States Patent No. 30,492.

[2] D. Godbole, J. Lygeros, E. Singh, A. Deshpande and A. Lindsey, "Design and verification of communication protocols for degraded modes of operation of AHS. ", *Proc. of the 34th IEEE Conference on Decision and Control,* New Orleans, LA, 1995. pp 427-432.

[3] R. Fenton, G. Melocik and K. Olson, "On the steering of automated vehicles: Theory and Experiment", *IEEE Trans. on Automatic Control,* vol. 21, no. 3, pp 306-315, 1976.

[4] W. Darenberg, "Automatische Spurführung von Kraftfahrzeugen (in German) ", Automobil-Industrie, pp 155-159, 1987.

[5] W. Zhang and R. Parsons, "An intelligent roadway reference system for vehicle lateral guidance/control", *Proc. American Control Conf.*, San Diego, CA, USA, 1990, pp 281-286

[6] S. Tsugawa, M. Aoki, A. Hosaka and K. Seki, "A survey of present IVHS activities in Japan", in *Preprints of the 13th IFAC World Congress (vol. Q),* San Francisco, CA, USA, 1996, pp. 147-152.

[7] Guldner J., Tan H., Patwardhan S., "Analysis of Automatic Steering Control for Highway Vehicles with Look-down Lateral Reference System", *Vehicle System Dynamics, special issue on Intelligent Vehicle Highway Systems (IVHS),* October 1996.